Journal of Hazardous Materials 476 (2024) 135134

Contents lists available at ScienceDirect

Journal of Hazardous Materials

journal homepage: www.elsevier.com/locate/jhazmat

# Fluorescent labeling of micro/nanoplastics for biological applications with a focus on “true-to-life" tracking

Aliro Villacorta [a,b,1], Camila Cazorla-Ares [c,1], Victor Fuentes-Cebrian [c], Iris H. Valido [c], Lourdes Vela [a,d], Fernando Carrillo-Navarrete [e], Michelle Morataya-Reyes [a], Karen Mejia-Carmona [f], Susana Pastor [a], Antonia Velázquez [a], Jéssica Arribas Arranz [a], Ricard Marcos [a], Montserrat López-Mesas [c,*], Alba Hernández [a,*]

[a] Group of Mutagenesis, Department of Genetics and Microbiology, Faculty of Biosciences, Universitat Autònoma de Barcelona, Cerdanyola del Vallès 08193, Spain
[b] Facultad de Recursos Naturales Renovables, Universidad Arturo Prat, Iquique, Chile
[c] GTS Research Group, Department of Chemistry, Faculty of Science, Universitat Autònoma de Barcelona, Cerdanyola del Vallès 08193, Barcelona, Spain
[d] Faculty of Health Sciences Eugenio Espejo, Universidad UTE, Quito, Ecuador
[e] Institut d'Investigació Tèxtil i Cooperació Industrial de Terrassa (INTEXTER) and Department of Chemical Engineering, Universitat Politècnica de Catalunya, Terrassa 08222, Barcelona, Spain
[f] Institut Català de Nanociència i Nanotecnologia (ICN2-UAB-CSIC-BIST), Cerdanyola del Vallès, Spain

## HIGHLIGHTS

- Advantages/disadvantages of five dyes to label nanoplastics (NPLs) were evaluated.
- A wide battery of assays was used for such determinations.
- iDye PolyPink was the dye showing more advantages.
- The advantages of labeling nano-polystyrene were extended to true-to-life NPLs.
- iDye PolyPink succeeded in staining titanium-dopped PET-NPLs.

## GRAPHICAL ABSTRACT

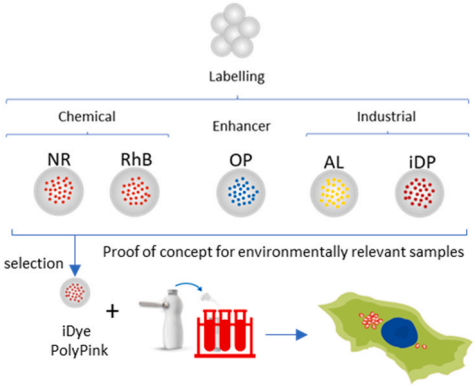


## ARTICLE INFO

*Keywords:*
Micro/nanoplastics
Staining
Specificity

## ABSTRACT

The increased environmental presence of micro-/nanoplastics (MNPLs) and the potential health risks associated with their exposure classify them as environmental pollutants with special environmental and health concerns. Consequently, there is an urgent need to investigate the potential risks associated with secondary MNPLs. In this context, using “true-to-life” MNPLs, resulting from the laboratory degradation of plastic goods, may be a sound approach. These non-commercial secondary MNPLs must be *labeled* to track their presence/journeys inside cells

* Correspondence to: Group of Mutagenesis, Department of Genetics and Microbiology, Faculty of Biosciences, and GTS Research Group, Department of Chemistry, Faculty of Science, both from Universitat Autònoma de Barcelona, Campus of Bellaterra, 08193 Cerdanyola del Vallès, Spain.
*E-mail addresses:* montserrat.lopez.mesas@uab.cat (M. López-Mesas), alba.hernandez@uab.cat (A. Hernández).
[1] Both authors contributed equally

https://doi.org/10.1016/j.jhazmat.2024.135134
Received 28 March 2024; Received in revised form 24 June 2024; Accepted 5 July 2024
Available online 8 July 2024

IDye PolyPink
Cell-internalization tracking

or organisms. Because the cell internalization of MNPLs is commonly analyzed using fluorescence techniques, the use of fluorescent dyes may be a sound method to label them. Five different compounds comprising two chemical dyes (Nile Red and Rhodamine-B), one optical brightener (Opticol), and two industrial dyes (Amarillo Luminoso and iDye PolyPink) were tested to determine their potential for such applications. Using commercial standards of polystyrene nanoplastics (PSNPLs) with an average size of 170 nm, different characteristics of the selected dyes such as the absence of impact on cell viability, specificity for plastic staining, no leaching, and lack of interference with other fluorochromes were analyzed. Based on the overall data obtained in the wide battery of assays performed, iDye PolyPink exhibited the most advantages, with respect to the other compounds, and was selected to effectively label "true-to-life" MNPLs. These advantages were confirmed using a proposed protocol, and labeling titanium-doped PETNPLs (obtained from the degradation of milk PET plastic bottles), as an example of "true-to-life" secondary NPLs. These results confirmed the usefulness of iDye PolyPink for labeling MNPLs and detecting cell internalization.

## 1. Introduction

Large-scale production of synthetic organic polymers can be traced back to the 1950′s. Since then, plastic production has progressively and steadily increased; consequently, a large amount of plastic waste has been continuously generated. Although environmental policies tend to reduce waste, a short-term scenario in which this situation could change is not feasible. In the environment, physicochemical or biologically mediated degradation processes of plastic waste produce secondary micro-/nanoplastics (MNPLs), which are considered environmental pollutants of emergent concern. Although the limits between microplastics (MPLs) and nanoplastics (NPLs) are still being investigated [1, 2], the smaller the size, the higher the probability of internalization into exposed organisms, including humans. As the definition of NPLs is a bit conflicting, this study considers NPLs in the range 1–1000 nm [3]. Multiple reviews have recently been published on the potential health risks associated with MNPL exposure, including oxidative stress, alterations in gene expression, genotoxicity, and carcinogenicity as potential effects associated with MNPL exposure [4-6]. However, the accurate determination of exposure (primarily at the NPLs level) requires further refinement and, consequently, the lack of exposure-effect information minimizes the relevance of the reported potential health risks [7]. In *in vitro/in vivo* experimental approaches, a growing interest exists in using "true-to-life" MNPLs resulting from the degradation of plastic goods because they are considered more representative of environmental plastic waste [3]. Accordingly, the use of these "true-to-life" MNPLs is a promising option, in opposition to the use of pristine polystyrene commercial MNPLs, to better define the potential risks associated with MNPL exposures owing to variations in their physicochemical properties. Notably, the confirmation that the used *"true-to-life"* (or any other used MNPLs) can internalize on cells/tissues should be a mandatory requirement in any published study. In this regard, significant advances have been made, pushing the boundaries of technology and techniques, demonstrating notable approaches such as the use of graphene oxide quantum dots to embed polystyrene (PS) microspheres by microemulsion polymerization [8] and hyperspectral imaging as a novel approach to studying the accumulation and distribution of NPs in human cells [9]. However, the development of techniques enabling three-dimensional (3D) analysis without detrimental or stressful effects at the cellular level and allowing, for instance, 3D reconstruction for future applications appears to be a secure path forward. Thus, it is necessary to "label" these *"true-to-life"* MNPLs in such a way that their presence can be easily detected to follow up on the presence of these plastics inside cell and /tissues. For such purposes, Nile Red staining has been extensively used to label MNPLs, showing multiple apparent advantages, including affordability and straightforward applications [10]. Although these advantages have been well-reported when environmental matrices are evaluated [11], problems arise with biological matrices [12], primarily because of the ability of Nile Red to stain intracellular lipid droplets/bodies. This ability to fluoresce strongly in lipophilic environments has been known for a long time and is why Nile Red was initially proposed to act as a lipid-specific stain [13]. In several cases, Nile Red has been used to detect propylene microplastics in crop plants; however, the protocol assumes the destruction/digestion of the plants, which prevents the detection of *in situ* internalization [14]. Using Nile Red staining, polystyrene, polyethylene, and polyamide were detected in the bottled water samples. In addition, when zebrafish embryos were exposed to Nile red-stained polyethylene MPLs, their accumulation was observed in various organs [15]. Therefore, owing to the non-specific staining ability of Nile Red and its high cost, more specific MNPL staining is required.

Several studies have determined the potential usefulness of alternative dyes such as textile dyes. In a recent study, four textile dyes (Rit pink, Rit blue, iDye pink, and iDye blue) were compared with Nile Red using 17 different polymers [16]. The results indicated the low efficacy of blue dyes and similar efficacy of pink dyes for Nile Red. Another study compared the usefulness of fluorescein and Nile Red in detecting polystyrene, polypropylene, and polyethylene MNPLs [17]. Significant differences between dyes were observed, with fluorescein enabling the specific detection of polystyrene, whereas Nile Red showed the highest increase in fluorescence for polypropylene. Unfortunately, all of these studies were carried out in water dispersions, but did not use biological matrices, as required for biological studies. Furthermore, Rhodamine B has been demonstrated to successfully stain five types of microplastic polymers (polyethylene, polypropylene, polystyrene, polyvinyl chloride, and polyurethane) under laboratory conditions [18]. In addition, polyvinyl chloride MPLs were successfully stained, and their ingestion was demonstrated in the copepod (*Pseudocalanus spp*) gut [19]. All these studies highlight the relevance of staining MNPLs and the lack of consistent proposals for one of them.

The lack of harmonized and established protocols for MNPL labeling, to detect cell internalization, is an important inconvenience in the development and study of the effects of "true-to-life" MNPLs. To fill this gap, the present study was conducted using two textile dyes (Amarillo Luminoso Polyester GNH 400 for industrial use and iDye PolyPink for domestic use), an industrial optical brightener (Opticol UPR), and two chemical dyes (Nile Red and Rhodamine B) to determine their suitability. The study consisted of two parts. In the first step, a suitable protocol for staining commercial polystyrene nanoplastics (PSNPLs) is developed, avoiding interference from other typical labeling fluorescence compounds; the stained-PSNPLs are internalized into cells and their distribution is studied. In the second one, and as a *proof of concept*, the selected dye, following a simplified staining protocol, was evaluated for the labeling of titanium-labeled PET nanoplastics (PET-Ti-NPLs) resulting from the degradation of opaque PET plastic bottles, followed by the internalization into cells [20]. As a novelty, our proposal for the best labeling method for MNPLs is based on a deeper analysis of the pros and cons of the five selected dyes after analyzing their responses in a wide battery of assays.

## 2. Materials and methods

### 2.1. Reagents and standards

Commercial standards of polystyrene nanoplastics (PSNPLs) were obtained from Ted Pella Inc. (Redding, CA, USA). These nanospheres had an SEM/TEM certified size of 170 ± 9 nm and were provided in an aqueous stabilized suspension (for non-aggregation purposes) at a concentration of 0.1 % (w/v). The selected compounds were Nile Red (NR), Rhodamine B (RhB) (Merck KGaA, Darmstadt, Germany), Amarillo Luminoso Polyester GNH 400 (AL), Opticol UPR (Op) (Colorcenter, Terrassa, Spain), and iDye PolyPink (iDP) (Rupert, Gibbon & Spider, Inc., Healdsburg, CA, USA). For the second part of the study, "true-to-life" PET(Ti)-NPLs obtained as described below were used. Briefly, 12 $cm^2$ fragments from commercially available milk PET bottles were sanded using a diamond rotary burr to avoid overheating the surface of the polymer. The debris was sieved through a 0.20 mm mesh and 4 g of the fine material was dispersed in 40 mL of 90 % (v/v) trifluoroacetic acid (TFA) pre-heated to 50 °C on a stirring plate at 100 rpm for 2 h, followed by continuous agitation at room temperature overnight. Particles in suspension were sieved through a 0.20 mm mesh, and the eluent was divided into 10 mL glass tubes and centrifuged for 1 h at 2500 rcf. The resulting pellet was resuspended in 400 mL of 0.5 % (v/v) sodium dodecyl sulfate (SDS) and subjected to ultrasonication using an SSE-1 Branson sonicator (Brookfield, CT, USA) for 2 min at 25 % amplitude, with 9/9 s sonication/break cycles, and immediately transferred to 200 mL graduated cylinders and allowed to sediment for 1 h to remove the larger fractions. The upper fraction (100 mL) of each cylinder was collected and centrifuged to remove SDS. The resultant pellets were washed twice with Milli-Q water and twice with pure ethanol, and dried under sterile air laminar flow. The dried pellets were weighed and resuspended in Milli-Q water at a concentration of 10 mg/mL. These suspensions were sonicated for 16 min at 10 % amplitude in a cold-water bath, immediately frozen using liquid nitrogen, and transferred to a − 80 °C freezer until needed.

### 2.2. Ultracentrifugation optimization

To achieve the highest centrifugation efficiency, a 40-ppm suspension of non-labeled PSNPLs was prepared in Milli-Q water. The suspension was ultracentrifuged for 5, 15, 30, or 45 min at 13,200 rpm using a 5415 R Eppendorf centrifuge (Eppendorf AG, Hamburg, Germany).

The centrifugation yield was determined using an ultraviolet-visible (UV-Vis) spectrophotometer (ATI-UNICAM UV2; Thermo Fischer, Braunschweig, Germany). This was calculated by comparing the intensity between the non-centrifuged suspension, used as a reference ($A_{250\ nm}$ *40 ppm standard*), and the supernatant of the centrifuged suspension at 250 nm ($A_{250\ nm}$ *(supernatant of centrifugation X min)*, which is within the range of the characteristic polystyrene wavelength, avoiding errors due to the saturation of the detector (Eq. 1).

$$Centrifugation\ Yield(\%) = \left(1 - \frac{A_{250nm}\quad (supernatant\ of\ centrifugation X \min)}{A_{250nm}\quad 40 ppm\ standard}\right)\cdot 100 \tag{1}$$

### 2.3. Membrane centrifugation efficiency study

To test another cleaning procedure, membranes Amicon® Ultra-15 centrifugal Ultracel®− 100 K filter $1 \times 10^5$ MWCO (Merck KGaA, Darmstadt, Germany) were tested. A calibration curve was prepared using concentrations ranging 150 ppt to 50 ppb of 170 nm PSNPLs, and the remaining PSNPL present in the eluent was calculated. Four replicates of the centrifugation procedure were performed for 15 min at 3500 rpm. The separation yield was calculated by measuring the absorbance (at 250 nm) of the membrane eluent and interpolating the values on the PSNPLs calibration curve corresponding to $y = 0.0197x + 0.0271$, $r^2 = 0.9959$, as detailed in the Supplementary Material (SEQ1).

### 2.4. Labeling procedure

All preparations were performed by separately weighing NR, RhB, AL, Op, and iDP to obtain a final stock concentration of 1000 ppm. The NR and RhB solutions were prepared using 96 % ethanol (Scharlab, Barcelona, Spain). For AL, Op, and iDP, the suspensions were prepared on "Ultrapure Type 1″ (Milli-Q) 18.2 MΩ·cm water (Merck KGaA, Darmstadt, Germany). PSNPLs at a fixed concentration of 40 ppm of PSNPLs was exposed to 400, 200, 100, and 50 ppm of each of the labeling solutions, regardless of water (AL, Op, and iDP) or 96 % ethanol (NR and RhB), as previously described. The different mixtures were heated at 65 ºC for 30 min on glass vials with constant agitation on an orbital agitator and incubator (Heidolph, Unimax1010) at 150 rpm. The stained particles were cleaned by performing ten ultra centrifugations for 45 min at 13,200 rpm, as described in the next section. The supernatant was removed from the pellet by decantation and further washes were performed with the corresponding solvent (Milli-Q water or ethanol, depending on the dye). The supernatants and resuspended pellets were analyzed using UV-Vis spectroscopy, as previously described, and fluorimetry analysis was performed. First, several concentrations of the strains were analyzed to determine the experimental excitation and emission wavelengths of each strain. Excitation fluorescence analysis was performed using a Cary Eclipse fluorescence spectrometer (Agilent, Santa Clara, CA, USA). Emission fluorimetry analysis was performed using the same parameters as in the excitation analysis; however, the initial scan wavelength was the excitation wavelength.

To study the cleaning efficiency, different supernatants were evaluated to determine the conditions that achieved the lowest possible fluorescence. Furthermore, to study the staining efficiency, the resuspended pellets of the stained PSNPLs were analyzed under the same conditions as previously described; however, the scan ranged from an excitation wavelength of 800 nm.

### 2.5. Agglomeration and resuspension study

To ensure that the agglomeration state of the stained PSNPLs remained negligible, the particles were heated at 65 °C for 45 min and ultracentrifuged for 45 min at 13,200 rpm ten times, reproducing the cleaning after the staining procedure. Subsequently, different resuspension procedures were applied to each one of the PSNPLs aliquots: no agitation (BC), orbital agitation (O) for 16 min at 350 rpm, vortex (V) for 16 min (Vortex-Vib, J.P SELECTA S.A., Barcelona, Spain), ultrasonic bath (BU) for 16 min (ULTR-3L2–001, Labbox Labware S.L, Barcelona, Spain), and ultrasonic probe (SU) at 10 % of amplitude for 16 min in a cold bath (SSE-1 Branson Sonicator, Branson Ultrasonics Co., Brookfield, CT, USA). The average size of the resuspended aliquots was analyzed by Dynamic Light Scattering (DLS) using a Zetasizer® Ultra (Malvern Panalytical, Cambridge, UK) and compared with a freshly prepared standard of 170 nm polystyrene nanospheres at 40 ppm. In all cases, size distribution was evaluated using a DTS0012 cuvette under the

conditions described in the following section. The data were processed and analyzed using GraphPad Prism software (GraphPad, San Diego, CA, USA).

### 2.6. The hydrodynamic behavior of labeled PSNPLs

The hydrodynamic behavior of the labeled PSNPLs was evaluated by measuring 100 ppm aliquots of labeled NPs in triplicate. To perform these measurements, the PSNPL parameters were established with a refractive index of 1.59. The parameters of Milli-Q water used as a dispersant were set as standards, considering a refractive index of 1.33 and a viscosity value of 0.8872. The sample size distribution was measured at a scattering collection angle of 174.7°using a DTS0012 cuvette, whereas the Z-potential was evaluated using DTS1070 cuvettes. The data obtained were analyzed as explained in the preceding section.

### 2.7. Cell culture

The THP1 leukemic monocyte cell line (Sigma-Aldrich) was selected based on its high ability to internalize MNPLs. Cells were maintained in filtered cap T-25 flasks (SPL Life Sciences, Pocheon-si, Gyeonggi-do, South Korea). The cellular suspensions were maintained at constant concentrations ranging 0.50–1.00 $\times$ $10^6$ cells/mL at a maximum volume of 5 mL on Roswell Park Memorial Institute (RPMI) medium supplemented with 10 % fetal bovine serum (FBS), 1 % glutamine (Biowest, Nuaillé, France), and 2.5 ppm of Plasmocin® (InvivoGen, CA, USA) at standard growing conditions of 37 ºC, on humidified atmosphere with 5 % $CO_2$, on a ICO150med $CO_2$ incubator (Memmert GmbH + Co KG, Schwabach, Germany).

### 2.8. Cell exposure to labeled PSNPLs

From the cell stock suspension, the required volumes at the concentration of 1.00 $\times$ $10^6$ cell/mL were distributed by seeding 100 µL per well on U-type 96-well plates (SPL, LifeSciences, Pocheon-si, Gyeonggi-do, Republic of Korea). The particle working suspensions, prepared as previously described, were mixed with the previously seeded cells by gentle pipetting ten times. The exposed cells were maintained under the same conditions as in the maintenance procedure for 24 h and protected from light. Based on a large number of studies using polystyrene NPLs, this nanoplastic can be considered stable over time. Although stability should be a problem in long-term exposure, this was not the case because the study used acute exposure lasting for 24 h.

### 2.9. Cell viability test

To avoid interference caused by nNPs in the standard viability tests, the direct scoring of the number of viable cells after exposure, compared to those before exposure, was determined using the Beckman counter method. THP1 cells were exposed to 100 ppm of differently stained particles following the procedure described above. The cell viability was investigated using a 1:100 ISOFLOW dilution on a ZTM Coulter Counter (Beckman Coulter Inc., CA. USA). The average cell count was compared with that of untreated controls, and values were analyzed using GraphPad Prism Software 7.0 (GraphPad, San Diego, CA, USA) by One-way analysis of variance (ANOVA) and contrasted with both unexposed and pristine-treated cells. For both cases the Dunnett post-test with a 95 % confidence interval (CI) with $p \leq 0.05$ (*), $\leq 0.01$ (**), and $\leq 0.001$ (***) was used. Two experiments were performed in triplicates.

### 2.10. Flow cytometry analysis

Cells treated with labeled particles and the labeling elute resulting from a previously indicated membrane centrifugation efficiency study were cultured as described in the cell viability test section. Cells in 96 U-type well plates were washed twice by centrifugation at room temperature on a 5810 R device (Eppendorf, Hamburg, Germany) and resuspended in phosphate-buffered saline (PBS; 1X, Gibco, Thermo Fischer Scientific, Braunschweig, Germany). The samples were kept on ice and immediately analyzed using a Cytoflex LX flow cytometer (Beckman Coulter Inc., CA, USA). The setting conditions were set as a standard, and the array/gain of the detectors can be found in the Supplementary Material (Supplementary Table S1). A total of 5000 living cell events were recorded at a flow rate of 60 µL/min. Data from the positive signal channels were analyzed and compared with the controls.

### 2.11. Confocal microscopy analysis

THP1 cells, treated with labeled particles and the particles labeling elute, as previously described, were cultured on U-type 96-well plates for 24 h. Cells were then washed twice using 200 µL of PBS 1X. Final pellet resuspension was done on a pre-warmed RPMI-supplemented medium, and 300 µL of the cell suspension was transferred to a well on a µ-Slide, eight-well high Glass bottom (Ibidi GmbH, Gräfelfing, Germany). The cells were examined using a Leica TCS SP5 confocal microscope (Leica Microsystems CMS GmbH, Mannheim, Germany). Compatibility was tested using CellMask™ deep red and trihydrochloride trihydrate Hoechst 3334 solution, both diluted 1:10,000 for all labels except for Opticol labeled PSNPLs, where the compatibility was changed to CellMasK Orange and DRAQ5 (Thermo Fischer Scientific, Braunschweig, Germany).

### 2.12. Simplified protocol and proof of concept

#### 2.12.1. Fast protocol

As the potential effects of PET-NPLs are gaining attention in the scientific community, a proof-of-concept study was performed following the protocol developed for PS. Instead of pristine PSNPLs, “true-to-life” PET(Ti)-NPLs were stained. These titanium-doped PETNPLs were obtained from the degradation, through sanding, of opaque PET bottles containing titanium NPs ($TiO_2$NPs); consequently, the resulting MNPLs also contained embedded titanium. Briefly, PET(Ti)-NPLs were labeled by mixing 0.5 mL of the PET(Ti)-NPL suspension (at a concentration of 10,000 ppm) with 0.5 mL of Milli-Q water (containing 0.01 g of iDye PolyPink) in a 10 mL glass tube. The mixture was vigorously agitated by vortex and incubated for 2 h with a short vortexing every 30 min on a constant temperature digital block heater (VWR® Avantor® Inc., Philadelphia, USA). The particle-label mix was resuspended in 9 mL of Milli-Q water and transferred onto an Amicon® Ultra-15 centrifugal Ultracel®− 100 K filter 1 $\times$ 10 5 MWCO (Merck KGaA, Darmstadt, Germany). A 15-min centrifugation was performed at 3453 rcf, and 9 mL of Milli-Q water was added to the V-shaped well; the wash was repeated four times. After washing, a volume ranging 100–160 µL containing the labeled particles was recovered from the V-shaped well and aliquoted to volumes of 1000 µL on Milli-Q water which were maintained covered from light at 4 ºC. Irrespective of the desired biological application, it is highly advisable to evaluate the effectiveness of this method by running a lambda scan on a regular confocal microscope for particle aggregates. Alternatively, approaches that do not necessarily rely on NP aggregation, such as fluorescent nanotracking analysis (NTA) or fluorescent spectrometry, can also be used. Both proposals employ widely used, cost-efficient, and easy-to-use approaches.

#### 2.12.2. Cell culture, treatment, and visualization

In this study, the human hepatic Huh-7 cell line was selected as a convenient experimental substitute for primary hepatocytes because the liver is one of the organs targeted by MNPLs pollutants. Huh-7 cells were cultured and seeded in filtered-cap T-25 flasks (SPL, Life Sciences Co. Ltd., Naechon-myeon, Republic of Korea) in Dulbecco’s modified Eagle’s medium (DMEM) supplemented with 10 % fetal bovine serum (FBS) from Biowest (Nouaillé, France) and Plasmocin (InvivoGen, CA, USA). To proceed, 7000 cells were seeded and cultured on µ-slide eight-

well high glass bottom (Ibidi GmbH, Gräfelfing, Germany) for 24 h before treatments. Culture media was removed by aspiration and replaced with 0.20 mL of freshly prepared iDye-PET(Ti)-NPLs suspension (100 μg/mL) on pre-warmed DMEM at 37 ºC and incubated for 24 h at standard growing conditions of 37 ºC, in a humidified atmosphere with 5 % $CO_2$ on an ICO150med $CO_2$ incubator (Memmert GmbH + Co KG, Schwabach, Germany). After 24 h of incubation with the iDye-PET (Ti)-NPLs suspension, cells were washed twice with 250 μL of a pre-warmed medium. Finally, 300 μL of pre-warmed medium was added to each well and the plates were investigated immediately after 5 min of incubation with CellMask™ deep red and trihydrochloride trihydrate Hoechst 3334 solution both diluted 1:10,000, on a Leica TCS SP5 confocal microscope (Leica Microsystems CMS GmbH. Mannheim, Germany).

## 3. Results and discussion

### 3.1. Ultracentrifugation optimization

First, ultracentrifugation conditions were established to separate PSNPLs from the supernatant. As expected, the results of centrifugation over time showed a significant decrease in the characteristic absorbance (at 250 nm) of PSNPLs (which indicated a decrease in the PSNPLs present in the supernatant) when the centrifugation time was increased (Fig. 1). The data indicate that the average intensity (absorbance in a.u.) decreased, from 2.69 at 0 min to 0.10 at 45 min. Consequently, the remaining PSNPL in the supernatant was reduced from 100 % at 0 min to 66 % at 5 min and to 4 % at 45 min of centrifugation. Consequently, 45 min was chosen as the optimal centrifugation time to separate the stained/unstained NPLs from the supernatant.

### 3.2. Membrane centrifugation efficiency study

As indicated in the Supplementary Information (Supplementary Fig. S1), the calibration curve for the analysis of PSNPLs showed a linear trend from 125 to 50 ppm. When using the calibration curve to evaluate the results from the four replicates performed with the Amicon® tubes, a concentration below the limit of detection was obtained. This indicates the non-significant presence of PSNPLs in the eluent, showing 100 % retention efficiency of the membrane used. However, when the PSNPLs were resuspended in the membrane, an average loss of 17 ± 8 % was observed. Therefore, this difference in absorbance can be attributed to the loss of particles stuck in the membrane or the walls of the tube, when trying to recover them from the membrane, after centrifugation. However, for the scope of the present study, membrane centrifugation was appropriate to ensure proper cleaning of the PSNPLs from the remaining staining in the supernatant when PSNPL labeling was used (see subsequent sections) to ensure separation from the supernatant in less time, even losing a higher amount. For subsequent analyses, the membranes were centrifuged whenever possible.

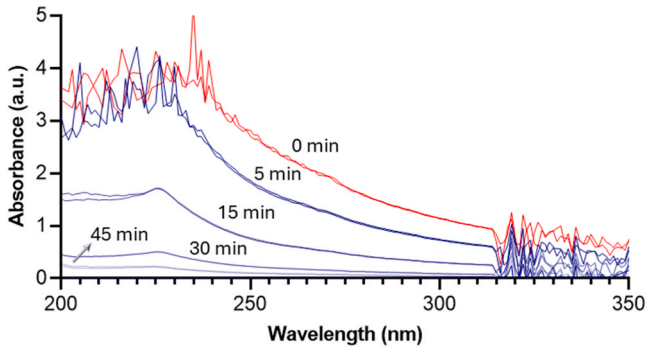


**Fig. 1.** The UV spectrum of each supernatant ranging 0–45 min of ultracentrifugation time at 13,200 rpm.

### 3.3. Staining and cleaning efficiency

To test the efficiency of the staining, different compounds were tested at different excitation and emission wavelengths, as shown in the Supplementary Material (Supplementary Table S2). The results obtained were within the range of those presented in the literature, except for Amarillo Luminoso and Opticol, for which no data were found in the open literature [21,22]. Regarding the fluorescence yield, the chemical dyes (NR and RhB) showed significantly higher fluorescence intensities, even at lower concentrations, than the textile dyes used and the optical brightener. Regarding the different concentrations of the dyes tested for labeling PSNPLs, the highest intensity in all resuspended PSNPLs was observed with the ratio corresponding to the highest concentration of the dye (corresponding to the ratio 10:1). Fig. 2 shows the emission spectra of the PSNPLs stained at 400 ppm, except for NR (200 ppm), which showed similar intensities.

Finally, concerning the cleaning of the PSNPLs to eliminate free dye, the procedures used were effective because the fluorescence intensity observed in the 10th wash supernatant was at least ten times lower than that of the stained PSNPLs. This fluorescence was colorless to the naked eye, except for NR and RhB, which showed a light red color with absorbance at the noise level when analyzed using UV-Vis spectrophotometry. Collectively, the results indicated that the ultracentrifugation cleaning procedure was reliable, and no free dye was detected in the visible spectrum at significant levels.

### 3.4. Agglomeration and resuspension study

The potential agglomeration levels of PSNPLs obtained using different resuspension approaches were evaluated by DLS and are graphically represented in Fig. 3a. The highest number of particles in all resuspension techniques had a diameter between 126–170 nm, which agreed with the results obtained in the blank of both DLS (named B) studies. The size distribution deviations were determined by considering the previously mentioned blank histograms (Fig. 3b). The ultrasonic probe exhibits the lowest deviation, followed by the ultrasonic bath, orbital, vortex, and centrifugation blanks.

The hydrodynamic behavior in terms of size distribution is depicted in Fig. 4 for all the stained particles evaluated. The Z-average values, based on intensity calculations, are 362 ± 5 nm for RhB, 363 ± 1 nm for AL, 309 ± 1 nm for Op, 352 ± 5 nm for iDP, and 539.50 nm for NR. The polydispersity indexes for 0.27, 0.25, 0.34, 0.62, and 0.70 for RhB, AL, OP, iDP, and NR, respectively.

The obtained size distributions were consistent, and for all cases (except NR), the Z-average values were close to 350 nm, showing solid correlation coefficients. Notably, the more reliable values for correlation

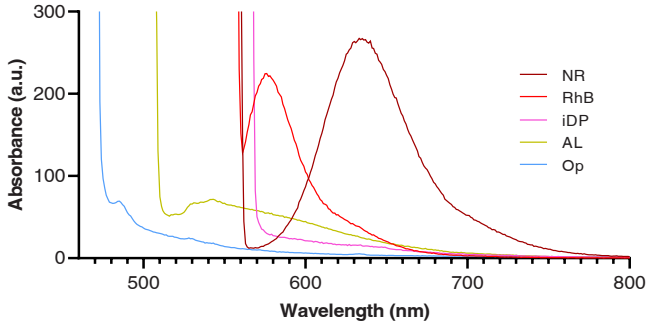


**Fig. 2.** Emission spectra of PSNPLs stained at 400 ppm (except for NR, which was stained at 200 ppm) with the different tested compounds. Legend abbreviations: Nile Red (NR), Rhodamine B (RhB), iDye PolyPink (iDP), Amarillo Luminoso (AL), and Opticol (Op).

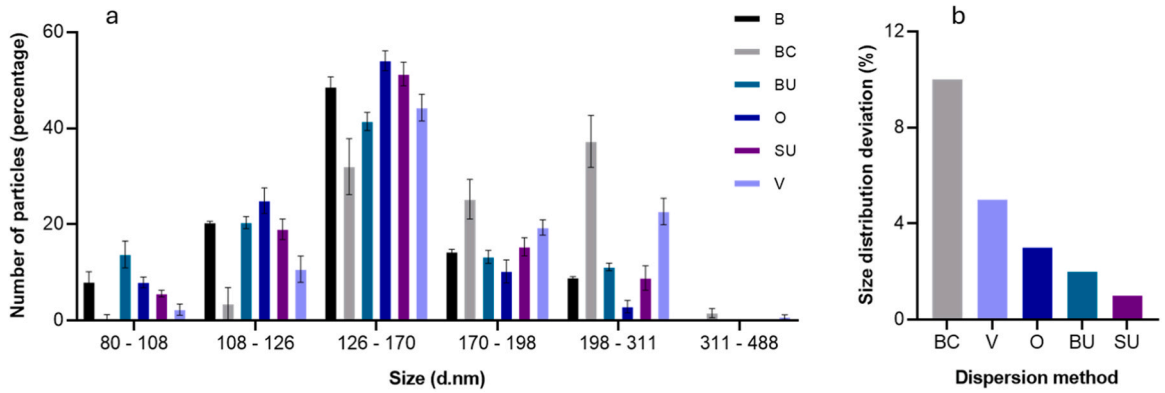


**Fig. 3.** (a) Size distribution histogram of the pristine PSNPL diameters obtained using DLS after different resuspension treatments. (b) Size distribution deviation expressed in percentages of the different resuspension techniques compared to the blank size distribution obtained using DLS. Legend abbreviations: DLS blank (B), centrifugation blank (BC), orbital (O), vortex (V), ultrasonic bath (BU), ultrasonic probe (SU).

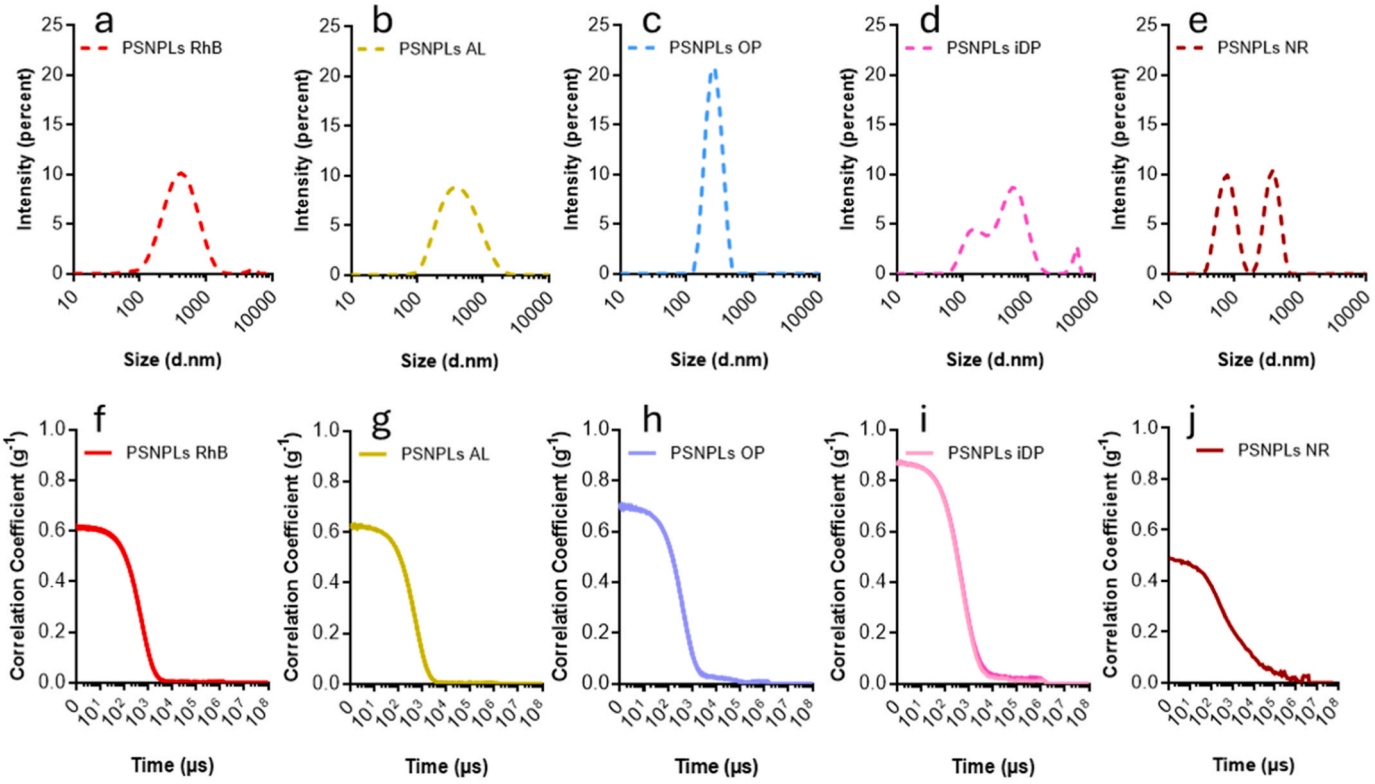


**Fig. 4.** Size distribution (using DLS) of PSNPLs for (a) RhB, (b) AL, (c) Op, (d) iDP, and (e) NR are represented as intensity percent. Correlation coefficients for all independent measurements are shown for RhB, AL, OP, iDP, and NR-stained PSNPLs on f, g, h, I, and j, respectively.

were those obtained when iDye PolyPink labeled particles were used, and the lower correlation was obtained for RhB and AL. In the case of NR-stained PSNPLs, the correlations and measurements were inconsistent and difficult to determine. These data indicate that the dispersion of iDye PolyPink-stained PSNPLs is the most suitable for future applications, especially if we consider that the typically described error in size estimation from fluorescent particles emitting in the range 600–700 nm is mild compared to Opticol, which is the only compound that does not emit in this range [23]. Even considering the relatively consistent values on the Z-average values, evidencing an agglomeration of particles related to the commercial information delivered by the manufacturer (170 ± 9 nm) the curves, for size distributions in percentage of intensity, describe the typically expected behavior for fluorescent samples. However, the fluorescent light emitted by some strains is non-coherent and can be recorded as noise, broadening the peaks [23]. This was observed for the RhB- and AL-stained NPs, which reduced their potential as candidates for labeling NPLs. With respect to the Z-potential, for all studied cases (Fig. 4a–d) the values were far from zero (summarized in Supplementary Table S3). Moreover, the values ranged − 20–(−46) mV which is an indicator that the suspensions are less prone to form aggregates. For RhB- and iDP-labeled NPLs, the measured values were close to − 30 mV, which is typically the optimum value for particles in suspension to be considered stable monodispersions.

### 3.5. Cell viability

A relevant condition for dye selection is that it should not compromise cell viability. In our study, no significant decrease in cell viability

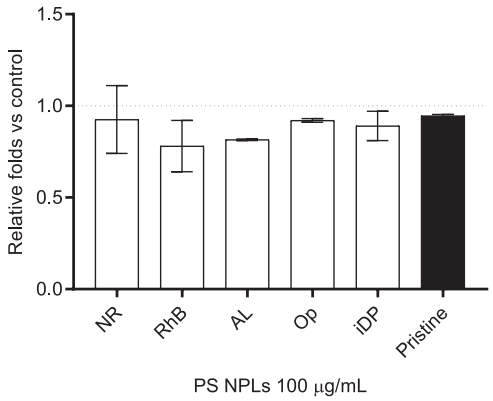


**Fig. 5.** Cell viability for THP1 cells after 24-h exposure to stained-PSNPLs. Nile Red (NR), Rhodamine B (RhB), Amarillo Luminoso (AL), Opticol (Op), and i-Dye Poly Pink (iDP) NPs (100 μg/mL). Values are relative to the untreated cells (control, dotted line). Cells treated with unlabeled PSNPLs (pristine) are also included. No significant statistical differences were observed using the one-side ANOVA with Dunnett's *post hoc* test ($p \leq 0.05$).

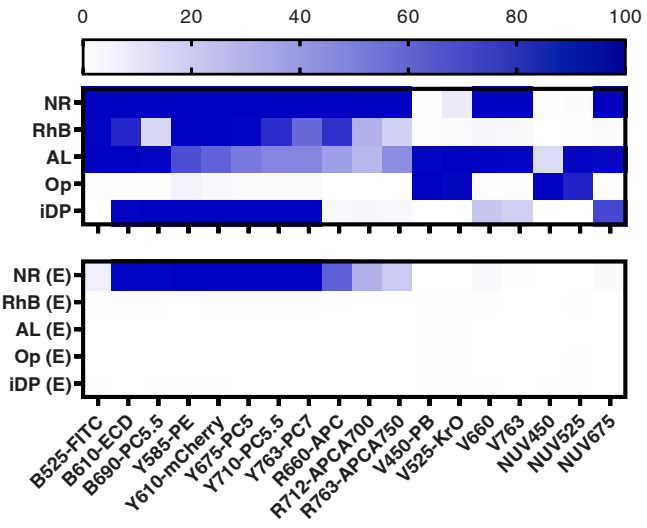


**Fig. 6.** Upper part: flow cytometry evaluation of the emission on THP1 cells exposed for 24 h to Nile red (NR)-, Rhodamine B (RhB)-, Amarillo luminoso (AL)-, Opticol (OP)-, and Idye PolyPink (iDP)-labeled polystyrene NPs (100 μg/mL). Lower part: data from their correspondent eluent (E-suffix added in all cases) for control. The used laser excitation and the corresponding wavelengths are indicated as follows: blue (B), yellow (Y), red (R), violet (V), and near UV (NUV). The emissions are represented as the percentage of cells that emit at the corresponding wavelengths.

was observed for any of the tested compounds in the human leukemia monocytic THP1 cells. This cell line has shown a significant ability to internalize PSNPLs [24], ensuring the uptake of labeled NPLs and supports the data indicating a lack of toxicity. However, small decreases in viability values were observed for RhB- and AL-stained PSNPLs; however, these decreases were not statistically significant, as indicated in Fig. 5. Notably, toxicity has been reported in A549 cells exposed to rhodamine-labeled silica NPs [25]. This means that the viability effects would not be a discriminating factor in the selection of the best compound to stain NPLs using this technique. However, it is tempting to advise against values deviating from the pointed line on the graph representing the values for untreated PSNPLs.

### 3.6. Flow cytometry analysis

The use of non-destructive techniques, such as fluorescence-activated cell sorting (FACS), may be favored by the fluorescent labeling of MNPLs. Therefore, the evaluation of its suitability with the selected strains may provide an idea as to which of the labels used in this study may be the most suitable. Thus, THP1 cells exposed for 24 h to labeled NPLs were investigated using flow cytometry. The details of each of the investigated channels are depicted in the Supplementary Material (Supplementary Figs. S2a–f for the particle-staining eluent, and Supplementary Figs. S2g–l for labeled particles). The first significant finding was the lack of specificity for Nile Red, which has already been discussed by other authors [26,27]. Thus, the high affinity of Nile Red for neutral lipids and other cellular components was demonstrated in our work. Despite previous reports on their usefulness, the use of Nile Red, as well as other stains with lipid affinity, should be considered a suboptimal approach when used in cellular backgrounds [20,28]. Thus, THP1 cells treated with different eluents showed no signal (Fig. 6), with the exception of the NR eluent. Therefore, these results would indicate both the effectiveness of the cleaning process and the inconvenience of using Nile Red. Thus, if we consider this characteristic crucial, the use of Nile Red must be discarded when better alternatives are available. Another characteristic is that no signal was detected near the UV spectra when Nile Red was in its free form or when no PSNPL particles were present.

For AL-PSNPL-treated cells, emission was observed in all channels, and the signal was mild (less than 25 %) only in the near ultraviolet (NUV)450 channel, where the shift was rounded to 13 %. Moreover, the shift was at least 50 % for 10 detectors. This may interfere with other signals emitted by other fluorochromes regularly used in biology as.

DRAQ5, Hoechst 33342 on nuclei, or Cellmask™ Deep Red for plasma membrane, and its use is inadvisable.

Moreover, because staining is persistent and difficult to remove, its inappropriate use may damage the microfluidic components of the cytometer. Notably, RhB- and iDP-labeled PSNPLs presented similar emissions, with the significant difference that internalized RhB-labeled PSNPLs emitted at 525 nm when excited with a blue laser and at 660 nm when excited with a red laser. In contrast, the internalized iDP-PSNPLs emit light at 675 nm when excited with an NUV laser. The differences between these two labels were minimal, and both results were almost equivalent. Finally, the Opticol-labeled PSNPLs presented a narrow emission spectrum (only at 450 and 525 nm) and only when excited with violet or near-UV lasers. Although Opticol appears to be useful in terms of compatibility, we will see further complications with this compound when complementary techniques are used. The results for RhB, iDP, and OP were confirmed and validated by repeating the experiments with adherent HeLa cells. These cells have been extensively used to study the effects of new materials, such as the label-free detection of metallic NPs [29], fluorescent nanopolymers [30], and carbon-based compounds [31]. Moreover, these cells have been supported by sophisticated techniques such as stimulated emission depletion microscopy, which is useful for detecting fluorescence at wavelengths lower than 200 nm [32]. Detailed methods and information on the use of this cell line are available in the Supplementary Material (Supplementary Figs. S3.1 and 2), and the comparisons are depicted and summarized in Supplementary Fig. S3.3.

### 3.7. Confocal microscopy

Internalization of the labeled NPs was assessed using confocal microscopy. For better visualization, despite the staining color, all labeled particles were represented in green, membranes in red, and nuclei in blue. Representative images of all the cases are shown in Fig. 7. The first observation (Fig. 7f) shows that Amarillo luminoso seems to produce not only interference with several of the signals but also causes some sort of cell stress, since in all cases, the shape of the cells was not regular and consistently altered compared to the control (Fig. 7g). Although cell viability was reduced in the short-term treatment (24 h), this reduction was not statistically significant. However, prolonged exposure may induce cell viability inconveniences that were not studied further

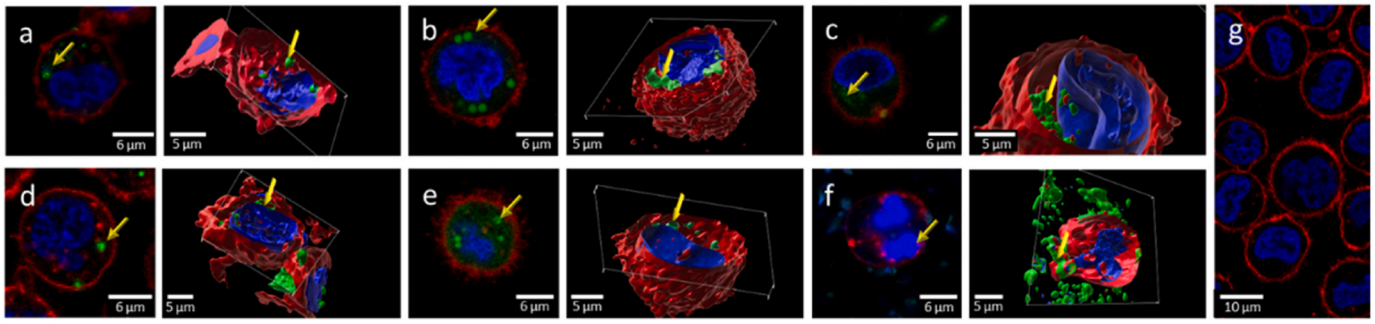


**Fig. 7.** Confocal Images of THP1 cells exposed for 24 h to commercially available (a) fluorescein labeled-PSNPLs, (b) Nile Red, (c) Rhodamine B, (d) Opticol, (e) i-Dye Poly Pink, and (f) Amarillo Luminoso PSNPLs (100 µg/mL). A digital reconstruction is presented at the right of each image. Yellow arrows indicate the presence of labeled NPs. Untreated THP1 cells are shown on (g), as controls.

because no useful traits for this label were found. Further experiments were not performed using this dye.

Although emissions at the expected wavelengths were easily observed, difficulties arose when the signals from small PSNPL agglomerates or single particles were evaluated. Although these difficulties can be solved using the so-called nanoscopy methodology, which is a far-field microscopy technique that can generate images beyond diffraction-limited resolution, such as stimulated emission depletion

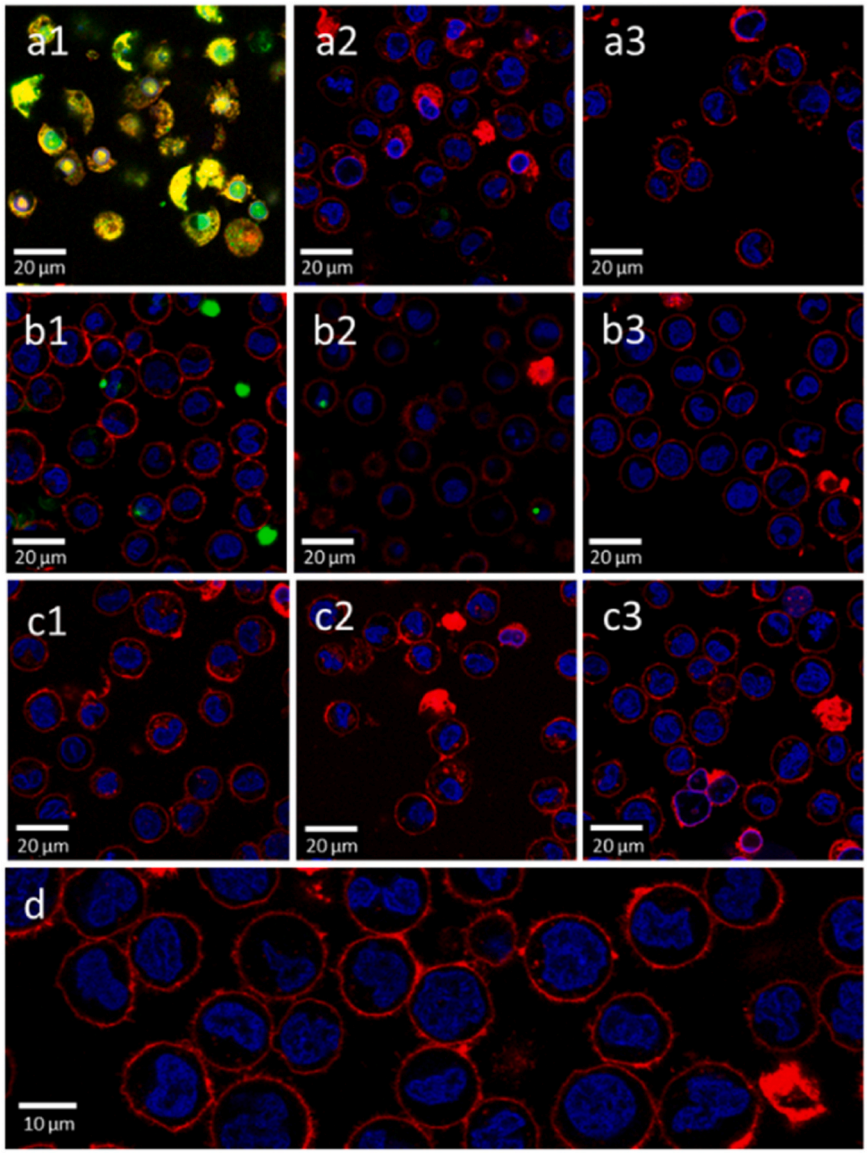


**Fig. 8.** Confocal Images of THP1 cells exposed for 24 h to pigments with no particles. (a1) Rhodamine B: 2000 ppm, (a2) 20 ppm, and (a3) eluent. (b1) Opticol: 2000 ppm, (b2) 20 ppm, and a(b3) eluent. iDye PolyPink: (c1) 2000 ppm, (c2) 20 ppm, and (c3) eluent. (d) Untreated THP1 cells.

(STED) microscopy [27], it can pose additional technical difficulties and a non-negligible increase in costs. In the case of NR-PSNPLs, owing to the previously explained non-specific staining, there are always uncertainties regarding the resulting images because the eluent can label the cells. Furthermore, since Nile Red presents an excitation wavelength shift from 450 to 560 nm by solvatochromism, its combined use with other stains or simultaneous scanning with B- and G-excitation filters may present scoring difficulties. No previous reports on RhB-labeled found in have been published. However, exposure to high concentrations of RhB may result in non-specific staining along with loss of cellular integrity, as shown in Fig. 8a1, whereas no signals were observed at low concentrations (20 ppm) or with the eluent (Fig. 8a2 and 3, respectively).

Although no effects on cell viability were observed when Opticol labeling was used, non-specific fluorescence signals were observed in THP1 cells treated with the particle-free stain, including high (2000 ppm) and low (20 ppm) concentrations (Fig. 8b1 and 8b2, respectively). However, the formation of Opticol hot spots was observed, suggesting the agglomeration of the compound. Furthermore, in agreement with the cytometry findings, no signals were detected in the eluent-treated cells (Fig. 8b3). As previously described, the compatibility of Opticol with regularly used stains permitted its use with DRAQ5 and CellMask Orange. Interestingly, the problems described for the previous two strains were not observed for the iDye PolyPink. Thus, no signals or detrimental visual effects on cell integrity were observed in any of the cases in which the cells were exposed to the iDye PolyPink dye or eluent (Fig. 8c1–3). Consequently, and for all the observations described above, we concluded that this labeling can be considered the most suitable alternative for tracking NPs on biological samples, not only because it does not generate cellular damage but also because it does not interfere with the channels used in confocal microscopy. Moreover, iDye-labeled PET and PS NPs have been reported to be used with Alexa Fluor 488 labeled secondary antibodies with no interference [33,34]. It has been also successfully proven to work well with fluorescent compounds used for cytometry-based mitochondrial potential detection [35] and FITC-marked antibodies for macrophage polarization detection[36]. This versatility in compatibility was difficult or impossible with previously published protocols that use covalently bound FITC emission labeling [37] because the emission cannot be used with regular markers used for intracellular reactive oxygen species detection, such as DHE or DCFH-DA, owing to the overlapping of signals.

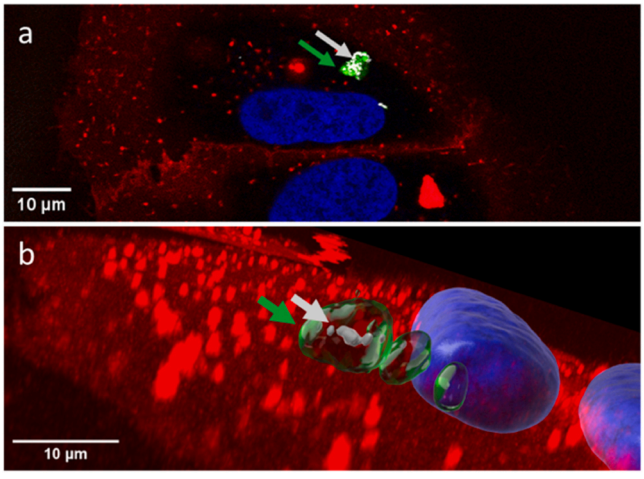


**Fig. 9.** (a) Confocal image of adherent Huh-7 cells exposed for 24 h to iDP-PET (Ti)NPLs. (b) 3D reconstruction of the image. Colocalization of Ti signal acquired through reflection (grey arrows) and labeled nano polymers-metal (green arrows).

### 3.8. Simplified protocol for staining and proof of concept

Based on the above results, we selected iDye PolyPink as the dye that offers advantages for staining NPLs. Since the previous work was carried out using pristine PSNPLs, to support the proposal, this study has been extended by using a "true-to-life" NPL model such as PET(Ti)NPLs, stained with iDP (particles called iDP-PET(Ti)NPLs from now on). These Ti-doped PETNPLs were obtained by degrading milk PET bottles [20] and their toxicological profile *in vivo has* recently determined in *Drosophila* [38]. Differentiated human hepatoma (Huh-7) cells were used for this study. These cells have a high ability to internalize NPs and present a wide set of biological responses [39]. Fig. 9 shows the results of the internalization of the iDP-PET(Ti)NPLs by Huh-7 cells, where the hybrid nature of the iDP-PET(Ti)NPLs was easily observed.

As demonstrated, the labeling of the PET moiety was always close to that of the doped titanium NPs, which is characteristic of PET opaque plastic. co-localization of the PET signal (labeled with iDP) and the reflection of Ti were visible in the interior of Huh-7 cells. This was always observed in the confocal images (as indicated in Fig. 9a), as well as in the 3D reconstruction (Fig. 9b), with a negligible background signal. This short study confirmed the effectiveness of the proposed simplified labeling protocol and its potential extension to other types of polymers and different cell types. Specifically, we determined the stability of the IDP labeling. Thus, IDP-labeled MNPLs were used after 8 months without the loss of fluorescence signals. This is another significant advantage of using the IDP.

Importantly, in parallel to this study, iDye PolyPink has been used to label different "true-to-life" nanoplastics aiming to confirm its advantages. Therefore, they have been used to label PET-NPLs resulting from the degradation of PET water bottles, PET(Ti)-NPLs from opaque milk bottles, and polylactic acid (PLA)-NPLs resulting from the release of PLA-teabags, when the process of simulating a cup of teabags. Thus, in *in vitro* studies, PET-labeled NPLs have been used to detect internalization into primary human nasal epithelial (HNEp) cells (Annangi et al., 2023). PET(Ti) labeled-NPLs have also been used to determine internalization in different hematopoietic cell lines, such as TK6 lymphoblasts, THP1 monocytes, and Raji-B lymphocytes [20]. Finally, iDye PolyPink was used to label NPLs from PLA bioplastics to determine their internalization into human intestinal cells such as Caco-2 and HT29, both as undifferentiated and differentiated cells, forming an *in vitro* model of the intestinal barrier [40]. Interestingly, iDye PolyPink labeling has been successfully applied to label PET and PET(Ti)-NPLs in an *in vivo* model, such as *Drosophila*, to demonstrate their uptake by enterocytes of the larval intestine or by hemocytes (with a function similar to lymphocytes in mammals) present in the hemolymph [38,41].

## 4. Conclusions

As a general conclusion of our study, iDye PolyPink is proposed as a potentially suitable dye to label MNPLs, especially those "true-to-life" resulting from the laboratory degradation of plastic goods of different chemical origins. The evaluation of both widely distributed commercially available PSNPLs and true-to-life nanopolymers confirmed the suitability of the proposed protocol for more complex samples. Noncommercial MNPLs require a robust labeling protocol to confirm their internalization in studies aimed at determining their potential hazardous biological effects. Accordingly, this study provides a detailed and simple protocol for labeling true-to-life MNPLs.

This selection of iDye PolyPink was based on the non-optimum behavior of the other selected dyes in different assays. Thus, 1) for Rhodamine-B, no clear supernatant was obtained, showing a certain effect on treated cell viability, nonspecific staining in confocal studies, and effects on cell integrity at high concentrations. 2) For Nile Red, a colored supernatant was observed despite the cleaning process. Furthermore, the lipophilic nature of the compound may induce nonspecific labeling in a lipid-rich environment, because lipid droplets

are present inside the cell. In such cases, a simpler method to separate the dyed plastic signal from nonspecific staining may be required. 3) Amarillo Luminoso had the clear characteristic of being detectable in all fluorescence investigated channels, which in turn makes its use for biological applications highly disfavored due to its compatibility with fluorophores that are used daily. 4) Opticol presented non-specific fluorescence inside and outside cellular structures, which may have resulted in misinterpretation of the results. Consequently, more complex approaches are required to verify the signals obtained from labeled particles.

In summary, the goodness and compatibility of iDye-labeled nanoplastics with the standardized techniques used to determine their presence in both cells and tissues make the present approach useful for the proposed objectives.

## Environmental implication

Environmental micro-/nanoplastics (MNPLs) are emerging pollutants of special concern, and determining their potential risks is essential. Although a large dataset has been obtained using pristine nanopolystyrene, it is not considered representative of the secondary MNPLs present in the environment. Consequently, obtaining true-to-life MNPLs resulting from the laboratory degradation of plastic goods seems to be an appropriate alternative to fill this gap. Notably, the use of such noncommercial MNPLs requires labeling to confirm their cell/tissue internalization. Although different dyes have been proposed for this purpose, there is a lack of comparative studies showing the advantages and disadvantages of each dye. In this study, after using a wide variety of assays to demonstrate their advantages and disadvantages, iDye Poly-Pink was proposed as the most suitable dye for labeling secondary MNPLs in studies aimed at identifying their internalization. Such labeling can be used in both in vivo/in vitro models to determine potential environmental and health hazards.

## CRediT authorship contribution statement

**Jéssica Arribas Arranz:** Methodology, Investigation. **Antonia Velázquez:** Supervision, Investigation. **Montserrat López-Mesas:** Writing – review & editing, Writing – original draft, Conceptualization. **Ricard Marcos:** Writing – review & editing, Conceptualization. **Michelle Morataya-Reyes:** Methodology, Investigation. **Fernando Carrillo-Navarrete:** Validation, Investigation. **Susana Pastor:** Supervision, Methodology, Investigation. **Karen Mejia-Carmona:** Supervision, Methodology. **Alba Hernández:** Writing – review & editing, Supervision, Conceptualization. **Victor Fuentes-Cebrian:** Validation, Investigation. **Camila Cazorla-Ares:** Validation, Investigation. **Lourdes Vela:** Validation, Methodology, Investigation. **Iris H. Valido:** Validation, Investigation. **Aliro Villacorta:** Writing – original draft, Methodology, Investigation.

## Declaration of Competing Interest

The authors declare that they have no known competing financial interests or personal relationships that could have appeared to influence the work reported in this paper.

## Data availability

Data will be made available on request.

## Acknowledgments

A. Villacorta was supported by PhD fellowships from the National Agency for Research and Development (ANID), from the CONICYT PFCHA/DOCTORADO BECAS CHILE/2020–72210237. L. Vela was supported by a Ph.D. fellowship from the Fundación Carolina. M. Morataya-Reyes hold a Ph.D. FI fellowship from the Generalitat de Catalunya. A. Hernández was granted an ICREA ACADEMIA award. I.H. Valido was supported by "Ayudas Margarita Salas para la formación de jóvenes doctores", Ministerio de Universidades (Spain).

This project has received funding from the European Union's Horizon 2020 Research and Innovation Programme under Grant Agreement No. 965196. This work was also partially supported by the Spanish Ministry of Science and Innovation [PID2020-116789, RB-C43], and by the Generalitat de Catalunya (2021-SGR-00731 and 2021-SGR-00723).

## Appendix A. Supporting information

Supplementary data associated with this article can be found in the online version at doi:10.1016/j.jhazmat.2024.135134.

## References

[1] Bhat, M.A., Gedik, K., Gaga, E.O., 2023. Atmospheric micro (nano) plastics: future growing concerns for human health. Air Qual Atmos Health 16 (2), 233–262. https://doi.org/10.1007/s11869-022-01272-2.

[2] Hartmann, N.B., Hüffer, T., Thompson, R.C., Hassellöv, M., Verschoor, A., Daugaard, A.E., et al., 2019. Are we speaking the same language? Recommendations for a definition and categorization framework for plastic debris. Environ Sci Technol 53 (3), 1039–1047. https://doi.org/10.1021/acs.est.8b05297.

[3] Villacorta, A., Rubio, L., Alaraby, M., López-Mesas, M., Fuentes-Cebrian, V., Moriones, O.H., et al., 2022. A new source of representative secondary PET nanoplastics. Obtention, characterization, and hazard evaluation. J Hazard Mater 439, 129593 https://doi.org/10.1016/j.jhazmat.2022.129593.

[4] Domenech, J., Annangi, B., Marcos, R., Hernández, A., Catalán, J., 2023. Insights into the potential carcinogenicity of micro- and nano-plastics. Mutat Res Rev Mutat Res 791, 108453. https://doi.org/10.1016/j.mrrev.2023.108453.

[5] Rubio, L., Marcos, R., Hernández, A., 2020. Potential adverse health effects of ingested micro- and nanoplastics on humans. Lessons learned from in vivo and in vitro mammalian models. J Toxicol Environ Health B Crit Rev 23 (2), 51–68. https://doi.org/10.1080/10937404.2019.1700598.

[6] Xu, J.L., Lin, X., Wang, J.J., Gowen, A.A., 2022. A review of potential human health impacts of micro- and nanoplastics exposure. Sci Total Environ 851 (Pt 1), 158111. https://doi.org/10.1016/j.scitotenv.2022.158111.

[7] Sohail, M., Urooj, Z., Noreen, S., Baig, M.M.F.A., Zhang, X., Li, B., 2023. Micro- and nanoplastics: contamination routes of food products and critical interpretation of detection strategies. Sci Total Environ 891, 164596. https://doi.org/10.1016/j.scitotenv.2023.164596.

[8] Liang, J.L., Cao, G.X., Zheng, F.Y., Li, S.X., Liu, F.J., Lin, L.X., et al., 2022. Low-toxic, fluorescent labeled and size-controlled graphene oxide quantum dots@ polystyrene nanospheres as reference material for quantitative determination and *in vivo* tracing. Chemosphere 307 (Pt 4)), 136094. https://doi.org/10.1016/j.chemosphere.2022.136094.

[9] Zhang, H.J., Zhou, H.R., Pan, W., Wang, C., Liu, Y.Y., Yang, L., et al., 2023. Accumulation of nanoplastics in human cells as visualized and quantified by hyperspectral imaging with enhanced dark-field microscopy. Environ Int 179, 108134. https://doi.org/10.1016/j.envint.2023.108134.

[10] Shruti, V.C., Pérez-Guevara, F., Roy, P.D., Kutralam-Muniasamy, G., 2022. Analyzing microplastics with Nile Red: emerging trends, challenges, and prospects. J Hazard Mater 423 (Pt B), 127171. https://doi.org/10.1016/j.jhazmat.2021.127171.

[11] Dutta, S., Misra, A., Bose, S., 2024. Polyoxometalate nanocluster-infused triple IPN hydrogels for excellent microplastic removal from contaminated water: detection, photodegradation, and upcycling. Nanoscale 16 (10), 5188–5205. https://doi.org/10.1039/d3nr06115a.

[12] Nalbone, L., Panebianco, A., Giarratana, F., Russell, M., 2021. Nile Red staining for detecting microplastics in biota: Preliminary evidence. Mar Pollut Bull 172, 112888. https://doi.org/10.1016/j.marpolbul.2021.112888.

[13] Greenspan, P., Fowler, S.D., 1985. Spectrofluorometric studies of the lipid probe, Nile Red. J Lipid Res 26, 781–789.

[14] Çelen Erdem, İ., Ünek, C., Akkuş Süt, P., Karabıyık Acar, Ö., Yurtsever, M., Şahin, F., 2023. Combined approaches for detecting polypropylene microplastics in crop plants. J Environ Manag 347, 119258. https://doi.org/10.1016/j.jenvman.2023.119258.

[15] Mohan, M., Gaonkar, A.A., Pandyanda Nanjappa, D., K.K, Vittal, R., Chakraborty, A., et al., 2023. Screening for microplastics in drinking water and its toxicity profiling in zebrafish. Chemosphere 341, 139882. https://doi.org/10.1016/j.chemosphere.2023.139882.

[16] Gao, Z., Wontor, K., Cizdziel, J.V., 2022. Labeling microplastics with fluorescent dyes for detection, recovery, and degradation experiments. Molecules 27 (21), 7415. https://doi.org/10.3390/molecules27217415.

[17] Aoki, H., 2022. Material-specific determination based on microscopic observation of single microplastic particles stained with fluorescent dyes. Sens (Basel) 22 (9), 3390. https://doi.org/10.3390/s22093390.

[18] Tong, H., Jiang, Q., Zhong, X., Hu, X., 2021. Rhodamine B dye staining for visualizing microplastics in laboratory-based studies. Environ Sci Pollut Res Int 28 (4), 4209–4215. https://doi.org/10.1007/s11356-020-10801-4.

[19] Le Quoc, P., Fokina, M.I., Martynova, D.M., Olekhnovich, R.O., Uspenskaya, M.V., 2022. Method of manufacturing and staining microplastics for using in the biological experiments. Environ Sci Pollut Res Int 29 (44), 67450–67455. https://doi.org/10.1007/s11356-022-22776-5.
[20] Villacorta, A., Vela, L., Morataya-Reyes, M., Llorens-Chiralt, R., Rubio, L., Alaraby, M., et al., 2023. Titanium-doped PET nanoplastics of environmental origin as a true-to-life model of nanoplastic. Sci Total Environ 880, 163151. https://doi.org/10.1016/j.scitotenv.2023.163151.
[21] Karakolis, E.G., Nguyen, B., You, J.B., Rochman, C.M., Sinton, D., 2019. Fluorescent dyes for visualizing microplastic particles and fibers in laboratory-based studies. Environ Sci Technol Lett 6 (6), 334–340. https://doi.org/10.1021/acs.estlett.9b00241.
[22] Maes, T., Jessop, R., Wellner, N., Haupt, K., Mayes, A.G., 2017. A rapid screening approach to detect and quantify microplastics based on fluorescent tagging with Nile Red. Sci Rep 7, 44501. https://doi.org/10.1038/srep44501.
[23] Bhattacharjee, S., 2016. DLS and zeta potential - what they are and what they are not. J Control Release 235, 337–351. https://doi.org/10.1016/j.jconrel.2016.06.017.
[24] Rubio, L., Barguilla, I., Domenech, J., Marcos, R., Hernández, A., 2020. Biological effects, including oxidative stress and genotoxic damage, of polystyrene nanoparticles in different human hematopoietic cell lines. J Hazard Mater 398, 122900. https://doi.org/10.1016/j.jhazmat.2020.122900.
[25] Gualtieri, M., Skuland, T., Iversen, T.G., Låg, M., Schwarze, P., Bilaničová, D., et al., 2012. Importance of agglomeration state and exposure conditions for uptake and pro-inflammatory responses to amorphous silica nanoparticles in bronchial epithelial cells. Nanotoxicology 6 (7), 700–712. https://doi.org/10.3109/17435390.2011.604441.
[26] Macairan, J.-R., Nguyen, B., Li, F., Tufenkji, N., 2023. Tissue clearing to localize microplastics via three-dimensional imaging of whole organisms. Environ Sci Technol 57 (23), 8476–8483. https://doi.org/10.1021/acs.est.2c07209.
[27] Nguyen, B., Tufenkji, N., 2022. Single-particle resolution fluorescence microscopy of nanoplastics. Environ Sci Technol 56, 6426–6435. https://doi.org/10.1021/acs.est.1c08480.
[28] Rodríguez-Hernández, A.G., Muñoz-Tabares, J.A., Aguilar-Guzmán, J.C., Vazquez-Duhalt, R., 2019. A novel and simple method for polyethylene terephthalate (PET) nanoparticle production. Environ Sci Nano 6 (7), 2031–2036. https://doi.org/10.1039/c9en00365g.
[29] Chithrani, B.D., Ghazani, A.A., Chan, W.C.W., 2006. Determining the size and shape dependence of gold nanoparticle uptake into mammalian cells. Nano Lett 6 (4), 662–668. https://doi.org/10.1021/nl052396o.
[30] Peñaloza, J.P., Márquez-Miranda, V., Cabaña-Brunod, M., Reyes-Ramírez, R., Llancalahuen, F.M., Vilos, C., et al., 2017. Intracellular trafficking and cellular uptake mechanism of PHBV nanoparticles for targeted delivery in epithelial cell lines. J Nanobiotechnol 15 (1). https://doi.org/10.1186/s12951-016-0241-6.
[31] Chaloupková, Z., Žárská, L., Belza, J., Poláková, K., 2023. Label-free detection and mapping of graphene oxide in single HeLa cells based on MCR-Raman spectroscopy. Anal Methods 15 (42), 5582–5588. https://doi.org/10.1039/d3ay01122d.
[32] Liu, Y., Peng, Z., Peng, X., Yan, W., Yang, Z., Qu, J., 2021. Shedding new lights Into STED microscopy: emerging nanoprobes for imaging (Frontiers Media S.A.). Front Chem Vol. 9. https://doi.org/10.3389/fchem.2021.641330.
[33] Annangi, B., Villacorta, A., Vela, L., Tavakolpournegari, A., Marcos, R., Hernández, A., 2023. Effects of true-to-life PET nanoplastics using primary human nasal epithelial cells. Environ Toxicol Pharmacol 100, 104140. https://doi.org/10.1016/j.etap.2023.104140.
[34] Annangi, B., Villacorta, A., López-Mesas, M., Fuentes-Cebrian, V., Marcos, R., Hernández, A., 2023. Hazard assessment of polystyrene nanoplastics in primary human nasal epithelial cells, focusing on the autophagic effects. Biomolecules 13, 220. https://doi.org/10.3390/biom13020220.
[35] Tavakolpournegari, A., Annangi, B., Villacorta, A., Banaei, G., Martin, J., Pastor, S., et al., 2023. Hazard assessment of different-sized polystyrene nanoplastics in hematopoietic human cell lines. Chemosphere 325, 138360. https://doi.org/10.1016/j.chemosphere.2023.138360.
[36] Tavakolpournegari, A., Villacorta, A., Morataya-Reyes, M., Arribas Arranz, J., Banaei, G., Pastor, S., et al., 2024. Harmful effects of true-to-life nanoplastics derived from PET water bottles in human alveolar macrophages. Environ Pollut 348, 123823. https://doi.org/10.1016/j.envpol.2024.123823.
[37] Magrì, D., Sánchez-Moreno, P., Caputo, G., Gatto, F., Veronesi, M., Bardi, G., et al., 2018. Laser ablation as a versatile tool to mimic polyethylene terephthalate nanoplastic pollutants: characterization and toxicology assessment. ACS Nano 12 (8), 7690–7700. https://doi.org/10.1021/acsnano.8b01331.
[38] Alaraby, M., Villacorta, A., Abass, D., Hernández, A., Marcos, R., 2024. Titanium-doped PET nanoplastics, from opaque milk bottle degradation, as a model of environmental true-to-life nanoplastics. Hazardous effects on Drosophila. Environ Pollut 341, 122968. https://doi.org/10.1016/j.envpol.2023.122968.
[39] Alsubaie, S.M., Ali, D., Almutairi, B.O., Almeer, R., Alarifi, S., 2022. Evaluation of cyto- and genotoxic influence of lanthanum dioxide nanoparticles on human liver cells, 15593258221128428 Dose Response 20 (3). https://doi.org/10.1177/155932582211284.
[40] Banaei, G., García-Rodríguez, A., Tavakolpournegari, A., Martín-Pérez, J., Villacorta, A., Marcos, R., et al., 2023. The release of polylactic acid nanoplastics (PLA-NPLs) from commercial teabags. Obtention, characterization, and hazard effects of true-to-life PLA-NPLs. J Hazard Mater 458, 131899. https://doi.org/10.1016/j.jhazmat.2023.131899.
[41] Alaraby, M., Villacorta, A., Abass, D., Hernández, A., Marcos, R., 2023. The hazardous impact of true-to-life PET nanoplastics in *Drosophila*. Sci Total Environ 863, 160954. https://doi.org/10.1016/j.scitotenv.2022.160954.